

# Classical-quantum localization in one dimensional systems: The kicked rotor

Cite as: AIP Advances 12, 035040 (2022); <https://doi.org/10.1063/5.0084028>

Submitted: 07 January 2022 • Accepted: 03 March 2022 • Published Online: 21 March 2022

 C. Hamilton and  J. Pérez-Ríos



View Online



Export Citation



CrossMark

## ARTICLES YOU MAY BE INTERESTED IN

[Effect of induced current loss on quality factor of graphene resonators](#)

AIP Advances 12, 035041 (2022); <https://doi.org/10.1063/5.0082259>

[Mechanism of development of turbulent boundary layer in a curved circular pipe under supersonic conditions](#)

AIP Advances 12, 035039 (2022); <https://doi.org/10.1063/5.0085586>

[Wave reversal mode in permalloy wire-tube nanostructures](#)

AIP Advances 12, 035044 (2022); <https://doi.org/10.1063/9.0000312>



Read Now!

AIP Advances  
Biophysics & Bioengineering Collection

# Classical-quantum localization in one dimensional systems: The kicked rotor

Cite as: AIP Advances 12, 035040 (2022); doi: 10.1063/5.0084028

Submitted: 7 January 2022 • Accepted: 3 March 2022 •

Published Online: 21 March 2022




View Online



Export Citation



CrossMark

C. Hamilton<sup>1</sup>  and J. Pérez-Ríos<sup>1,2,a)</sup> 

## AFFILIATIONS

<sup>1</sup>Fritz-Haber-Institut der Max-Planck-Gesellschaft, Faradayweg 4-6, 14195 Berlin, Germany

<sup>2</sup>Department of Physics and Astronomy, Stony Brook University, Stony Brook, New York 11794, USA

<sup>a)</sup>Author to whom correspondence should be addressed: [jesus.perezrios@stonybrook.edu](mailto:jesus.perezrios@stonybrook.edu)

## ABSTRACT

This work explores the origin of dynamical localization in one-dimensional systems using the kicked rotor as an example. In particular, we propose the fractal dimension of the phase space as a robust indicator to characterize the onset of classical chaos. As a result, we find that the system crosses the stability border when the fractal dimension  $\geq 1.81$ , and we obtain a functional form for the fractal dimension as a function of the kick strength. At the same time, dynamical localization is explored in the quantum realm by looking into the energy-localization relationship across the classical stability border, thus finding a correlation between the classical chaos and the presence of dynamical localization.

© 2022 Author(s). All article content, except where otherwise noted, is licensed under a Creative Commons Attribution (CC BY) license (<http://creativecommons.org/licenses/by/4.0/>). <https://doi.org/10.1063/5.0084028>

## I. INTRODUCTION

The kicked rotor is a traditional system in theoretical physics to study the fundamentals of classical and quantum chaos. In particular, it is a crucial system for the study of dynamical systems since it shows stochastic motion, as explained by Chirikov<sup>1</sup> and Greene.<sup>2</sup> Moreover, the kicked rotor has been employed on the quantal front (the quantum kicked rotor) to study the nature of quantum chaos and its relationship with classical chaos due to its analogy with the standard map. As a consequence, a vast amount of literature has been published treating different facets of the quantum kicked rotor, such as the quantum suppression of classical diffusion, also known as dynamical localization,<sup>3–5</sup> the localization of the wave function,<sup>6,7</sup> which is somehow related to the Anderson localization,<sup>8,9</sup> or the existence of quantum resonances in which the energy of the system grows faster in time than in the classical case.<sup>3,10–12</sup> In fact, some of the theoretical predictions have been corroborated by experimental realizations that usually come in two flavors: (i) atoms and molecules in microwave fields<sup>13,14</sup> and (ii) ultracold atoms in pulsed optical lattices.<sup>15–23</sup>

The quantum mechanical version of a classically chaotic system generally shows the expected repulsion of energy levels. In most cases, spectral properties can be described by random matrix

theory, following one of the possible ensembles based on the symmetries of the system under consideration.<sup>24–31</sup> However, the quantum kicked rotor shows a quasi-energy spectrum rather than an energy spectrum since it is a time-dependent system and energy is not a conserved quantity. Furthermore, and surprisingly enough, its quasi-energy spectrum is regular (follows a Poisson distribution) due to the exponential localization in momentum space characteristic of the system. Consequently, the onset of quantum chaos is not well described by random matrix theory. Instead, dynamic localization is mainly used to characterize the onset of quantum chaos, which is believed to be a quantum interference effect due to its similarity with Anderson localization.<sup>8,9</sup> However, recent studies challenge that interpretation and still the nature of dynamical localization is under debate.<sup>32–34</sup>

This paper presents a study on the classical-quantum correspondence in one-dimensional systems in light of the dynamical localization using the kicked rotor as a prototypical example. First, we propose using the fractal dimension of the phase space as the parameter to specify the onset of classical chaos since it is naturally related to the phase space volume that exhibits stochastic diffusion. Second, the relation between the average energy and the localization of the wave function is analyzed in the transition from ordered to

diffusive classical regimes, thus giving new insights into the nature of the dynamical localization.

This paper is organized as follows: Sec. II introduces the fractal dimension of the phase space as the parameter to specify the onset of classical chaos. Then, Sec. III explores the classical-quantum correspondence of the dynamical localization in the quantum kicked rotor. Finally, Sec. IV contains a summary and main conclusions drawn from the present study.

## II. FRACTAL DIMENSION AS A MEASURE OF CLASSICAL CHAOS

Fractals and chaos are related at a fundamental level. One of the necessary conditions a system must have to be chaotic is exponential sensitivity to the initial conditions.<sup>35</sup> Because of this property, when looking into the phase space of a chaotic system, we can expect trajectories to pass extremely close to one another in some areas of the phase space and to be more spread out in other areas. This diverging behavior is present at arbitrarily small scales, as even tiny differences in initial conditions will eventually diverge in chaotic systems. As the defining property of fractals is the fine structure that persists at arbitrarily small scales,<sup>36</sup> we can thus expect the phase space of a chaotic system to be a fractal.

A prime example of a chaotic system showing a fractal nature is the dynamics of ultracold dipolar collisions.<sup>37</sup> In such a system, it has been shown that the emergence of quantum chaos is connected to the volume of phase space presenting a chaotic (or fractal) nature. Similarly, in two-dimensional (2D) maps, it has been shown that the area covered by chaotic orbits in phase space depends on the resolution to measure it, and they are called fat fractals.<sup>38</sup> However, the concept of fat fractal seems to contradict *a priori* Newhouse's theorem about the integral dimension of strange attractors.<sup>39</sup> Although, they can be reconciled by considering that Newhouse's theorem is a formal result applicable to a complete orbit with infinite points. In contrast, the concept of fat fractals emerges as a numerical exploration of two-dimensional maps, including a large but finite number of points. Therefore, from a numerical perspective, the fractal properties of chaotic orbits can be treated as effective rather than apparent.

Fueled by these results and following previous studies on the nature of classical chaos of the kicked rotor,<sup>40,41</sup> we propose to use the fractal dimension as a measure of classical chaos. The fractal dimension measures the detail present in a curve at increasingly small scales. The more the chaotic system, the more the trajectories in phase space will diverge from one another at smaller distances, and so the level of detail at smaller scales will be higher, and thus, the fractal dimension of the phase space will be greater.

Here, we chose the box-counting dimension or the Minkowski–Bouligand dimension<sup>42</sup> to characterize the fractal dimension as it is elaborated in Appendix A. As with all fractal dimensions, the box-counting dimension is a measure of how the detail of a set of points varies as a function of scale. The Hamiltonian of the classical kicked rotor is given by

$$\mathcal{H}(L, \theta; t) = \frac{L^2}{2I} + \mu\epsilon_0 \cos \theta \sum_{n=0}^{\infty} \delta\left(\frac{t}{T} - n\right), \quad (1)$$

which describes the dynamics of a 2D rotor in a time-dependent electric field.  $\delta(x)$  denotes the Dirac delta function of argument

$x$ , and the infinite sum of Dirac delta functions is associated with a comb of kicks that describe the periodic kicks of the system. In Eq. (1),  $L$  is the angular momentum,  $I$  is the moment of inertia,  $\mu$  is the dipole moment of the rotor,  $\epsilon_0$  is the electric field strength,  $\theta$  is the angle between the external electric field and the axis of the rotor, and  $T$  is the period of the kicks. After applying Hamilton's equations and simplifying the results, we are left with the standard mapping,

$$\begin{aligned} l_{n+1} &= l_n + K \sin \theta_n, \\ \theta_{n+1} &= \theta_n + l_{n+1}, \end{aligned}$$

where the dimensionless angular velocity and angle immediately before the  $n$ th kick are denoted by  $l_n$  and  $\theta_n$ , respectively, and  $K \equiv \mu\epsilon_0 T^2/I$ . As both equations of the standard mapping are invariant to addition of multiples of  $2\pi$ , the phase space can be projected onto a torus.

Phase space diagrams are obtained for different values of  $K$  by iterating the standard map of the kicked rotor and plotting the angular momentum vs the angle for each of the iterations. The phase space diagrams have been calculated by using 100 initial trajectories each propagated with  $10^4$  time steps. As already argued, we expect the phase space diagram of a chaotic system to be a fractal, so we calculated the fractal dimension for the phase space diagrams for the different values of  $K$ , as shown in Fig. 1. This figure shows that the fractal dimension varies between 1 and 2, as expected. A fractal dimension of 1 correlates with a line in the phase space, i.e., uniform motion of the system without interaction potential. On the contrary, a fractal dimension of 2 implies a fully chaotic phase space or the absence of stability regions. However, a fractal dimension of 2 cannot be attained since there are always narrow stable regions for  $K \gg 1$ , as explained in Ref. 1.

To better illustrate the relation between fractal dimension and  $K$ , we show a few characteristic phase space diagrams for different values of  $K$  (see the insets of Fig. 1). As a result, we note a growth of the dense unstable regions of motion in correlation with the values of  $K$ . In particular, the larger the stable regions are, the lower the fractal dimension is, thus confirming its value as a parameter for the characterization of the onset of chaos. Furthermore, it is clear that there is a plateau around  $K \approx 0.5$  and then a steep rise around  $K \approx 1$ , before plateauing again for  $K > 1.5$ . This behavior may be correlated with the width of the stochastic layer for the stability border around  $K \approx 1$ .

The literature analyzing the classical kicked rotor often focuses on the region around  $K_{cr} \approx 0.97$ : the lowest value of  $K$  such that there is no invariant non-resonant curve spanning all angles<sup>6</sup> or the value often considered as the stability border following the Kolmogorov–Arnold–Moser (KAM) theory.<sup>43,44</sup> Then, using the fact that  $K \approx 1$  is the tipping point, the steep curve of the fractal dimension around  $K \approx 1$  shows the transition from stable to globally unstable or chaotic. In general, we find that the box-counting dimension is different from the topological dimension of the phase space, thus confirming its fractal nature. For  $0.5 \lesssim K \lesssim 2.0$ , we find that the box-counting dimension can be heuristically described by

$$D(K) = \alpha \tanh(\beta K + \gamma) + \delta, \quad (2)$$

and the results are depicted by the red line in Fig. 1. Moreover, the same expression explains the fractal dimension of a chaotic orbit in phase space of other two-dimensional maps.<sup>41</sup> It is interesting

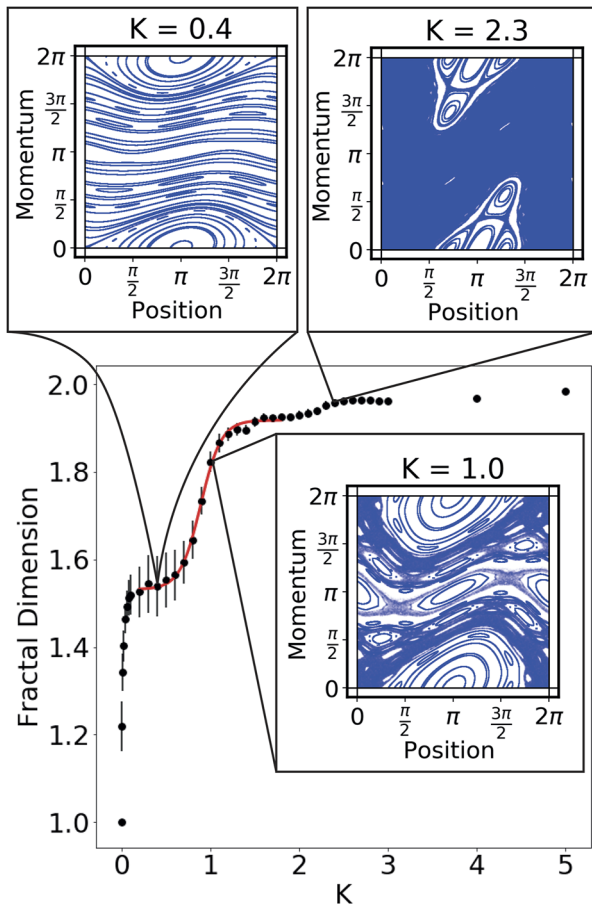


**FIG. 1.** Fractal dimension as a function of the classical parameter  $K$  for the classical kicked rotor. Each point shows the corresponding error bar based on the box-counting method as explained in Appendix A. The red line corresponds to the fitting of Eq. (2). The insets show the phase space for different values of  $K$  (shown in the top of each panel).

to note that the upper limit of  $K$  for which Eq. (2) is applicable roughly corresponds to the stability border based on the overlap criterion. Similarly, the lower limit,  $K = 0.5$ , corresponds to a scenario in which 96% of the trajectories are stable.<sup>1</sup> In particular, after fitting our results to Eq. (2), we find  $\alpha = 0.194 \pm 0.003$ ,  $\beta = 4.298 \pm 0.263$ ,  $\gamma = -3.820 \pm 0.239$ , and  $\delta = 1.725 \pm 0.003$ . The onset of classical chaos identifies with a fractal dimension of 1.81. In other words, as long as the system is chaotic, its fractal dimension is bounded and given by  $D \geq 1.81$ . Consequently, different realizations of the kicked rotor are very close to each other when analyzing the fractal dimension of the phase space.

### III. DYNAMICAL LOCALIZATION: FROM ORDER TO DIFFUSIVE REGIMES

The Hamiltonian of the quantum kicked rotor reads as<sup>45</sup>

$$\hat{H} = \frac{\hat{L}^2}{2I} + \mu\epsilon_0 \cos \theta \sum_{n=0}^{\infty} \delta\left(\frac{t}{T} - n\right), \quad (3)$$

where  $\hat{L}$  represents the angular momentum operator in 2D. After using the time-dependent Schrödinger equation to determine the evolution of the system, two dimensionless control parameters are found,  $\tau \equiv \hbar T/I$ , where  $\hbar$  is the reduced Planck constant, and  $k \equiv \mu\epsilon_0 T/\hbar$ . The former is connected to the free evolution of the rigid rotor between kicks, whereas the latter is with the kick itself. The product of these quantal parameters leads to the parameter relevant for the onset of classical chaos,  $K = k\tau$ .

Let us assume that the state of the system in momentum space at a given time,  $t$ , is given by the ket  $|\psi(t)\rangle$ ; then, the evolution of the system after one period is given by

$$|\psi(t+T)\rangle = \hat{U}(k, \tau)|\psi(t)\rangle, \quad (4)$$

where  $\hat{U}$  is the evolution operator over one period. In momentum space, the wave function is described as

$$|\psi(t)\rangle = \sum_{n=-l}^l c_n(t)|n\rangle, \quad (5)$$

where  $|n\rangle$  denotes the  $n$ th momentum state, and the evolution operator is given by a  $(2l+1) \times (2l+1)$  matrix representation,<sup>6</sup>

$$U_{nm}(k, \tau) = e^{i\frac{\tau}{4}(n^2+m^2)} e^{i\frac{\tau}{2}(n-m)} J_{n-m}(k), \quad (6)$$

where  $J_n(k)$  is a Bessel function of the first kind of order  $n$ . Within such a representation,  $\tau$ , unlike  $k$ , only changes the phase and not the magnitude of the elements of the matrix, so  $\tau$  will not affect the number of basis states needed to ensure unitarity of the evolution operator; only  $k$  determines that. The further from the main diagonal, the larger the order of the Bessel function, and the smaller the matrix element is there. The larger the  $k$ , the more the terms farther from the main diagonal we need to include. As a result, the number of momentum states required for an accurate description of the dynamics depends on the value of  $k$ , as is elaborated in Appendix B. In particular, for  $k = 0.5$ , the momentum ranged from  $l = -250$  to 250, and for  $k = 4$ , the momentum ranged from  $l = -2250$  to 2250.

It is well-known that the quantum kicked rotor shows dynamical localization,<sup>3-5,8,9</sup> i.e., the quantum suppression of classical diffusion, as explained in Sec. I. In general, dynamical localization is almost identical to the Anderson localization once a proper map is introduced. Therefore, dynamical localization is a consequence of quantum interference, although recent studies show that dynamical localization appears only when the classical counterpart present a chaotic behavior.<sup>32-34</sup>

Assuming localization of the wave function, the probability of finding the kicked rotor in a given momentum state  $x$  is  $P(x, \lambda) \propto e^{-\frac{|x|}{\lambda}}$ , where  $\lambda$  is the localization length; the smaller the  $\lambda$ , the more localized it is. To properly describe a probability,  $P(x, \lambda)$  needs to be discretely normalized, leading to

$$P(x, \lambda) = \tanh\left(\frac{1}{2\lambda}\right) e^{-\frac{|x|}{\lambda}}. \quad (7)$$

On the other hand, the energy of the system is given by

$$E = \langle \psi | \frac{\hat{L}^2}{2} | \psi \rangle = \frac{1}{2} \sum_{n=-\infty}^{\infty} n^2 P(n), \quad (8)$$

where  $P(n)$  denotes the probability to find the system in a state of given momentum  $n$ . Then, assuming that such probability is given by Eq. (7), we find

$$E(\lambda) = \frac{1}{4} \left[ \operatorname{csch}\left(\frac{1}{2\lambda}\right) \right]^2, \quad (9)$$

which only depends on the localization length. Therefore, the localization length and energy are intimately related, as it has been discussed previously in the literature.<sup>6</sup> Indeed, Eq. (7) is strictly valid for  $x \gg 1$ , i.e., for the description of the tail of the probability density function.<sup>6</sup> Hence, Eq. (9) is only an approximation to the expected energy of the system. Equation (9) can be well approximated by  $E(\lambda) \approx \lambda^2$ , as the first two terms of the Laurent series of Eq. (9) are  $\lambda^2 - \frac{1}{12}$ . We thus expect the energy to roughly scale with the square of the localization length (this relationship has been discussed previously in other papers, such as Ref. 6).

To further explore the relation between the localization length and average energy beyond any previous work, we ran simulations for various values of  $k$  and  $\tau$ . In particular, we choose 50 different values of  $K \in [0.1, 5]$ , and for each of these values, we pick 15 different values of  $k \in [0.5, 4]$  and  $\tau \in [0.025, 10]$  to keep  $K = k\tau$  fixed. We, thus, have  $50 \times 15 = 750$  simulations of different systems. For each of the 15 realizations associated with a given value of  $K$ , on the one hand, we calculate the average energy  $\langle E \rangle$  resulting from averaging the energy of the system during 450 time steps once the system reaches a steady-state, which takes of the order of 50 time steps. On the other hand, we calculate  $\langle \lambda^2 \rangle$  by averaging the square of the localization length for 150 time steps after 350 time steps, thus ensuring that the system's state has had enough time to visit all the accessible momentum states.

The results are displayed in Fig. 2 where  $\langle E \rangle$  is plotted vs  $\langle \lambda^2 \rangle$  for four different values of  $K$  or  $D$ . This figure shows a correlation between the energy and the square of the localization length: the larger the localization length, the larger the energy is. A behavior expected in virtue of the role of the diffusion of momentum in classical chaotic regions. In particular, the relationship between those magnitudes is linear, and it is fulfilled for values of  $D \geq 1.54$ .

Furthermore, we realize that even though the relation between the energy and the square of the localization length is mainly linear, the slope has a severe dependence on  $K$ , or  $D$ , as it is shown in Fig. 3. This figure displays the slope, including its error when fitting the averaged energy as a linear function of  $\langle \lambda^2 \rangle$ . In particular, one notes that the slopes decrease with increasing  $D$ , showing an abrupt change between  $D = 1.81$  and  $D = 1.93$ , corresponding roughly with the classical stability border. A more precise analysis is displayed in the inset of Fig. 3, where the same magnitude is shown in a semi-log plot, exhibiting two distinct trends: A cubic dependence on the classical stable region and a flat dependence beyond the classical stability border. The exact point of the transition between those trends lies in the shaded area depicted in the inset. The results in Fig. 3 corroborate previous studies pointing out the necessity of being in a classical chaotic regime to observe dynamical localization.<sup>32,33</sup> Furthermore, it seems that the average energy vs the squared localization length is a suitable parameter for defining the onset of quantum chaos in the quantum kicked rotor. Indeed, this parameter will be the equivalent of  $D$  or  $K$  but from the quantum mechanical front.

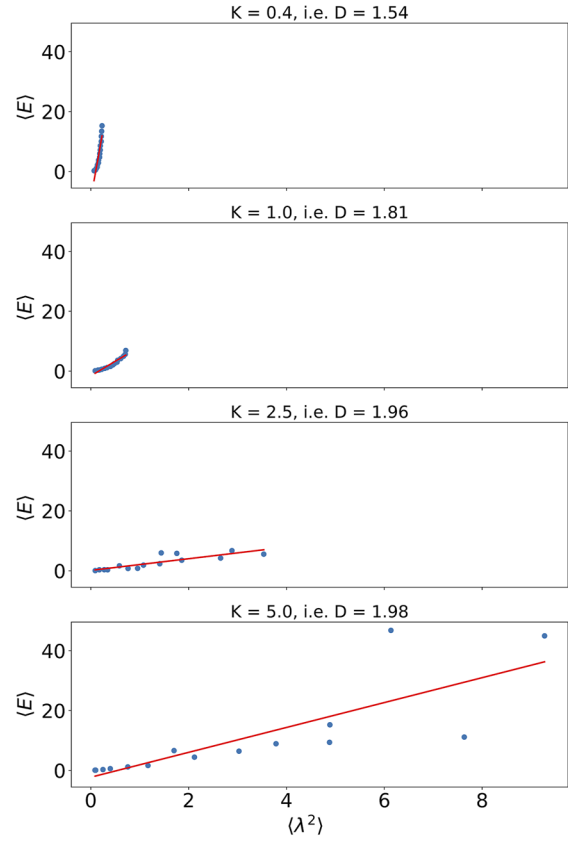


FIG. 2. Energy vs average localization length for different values of  $K$  (the corresponding  $D$  values are also shown). Each of the panels contains 11 realizations of the system with different values of  $k$  and  $\tau$  so as to keep  $K = k\tau$  fixed.

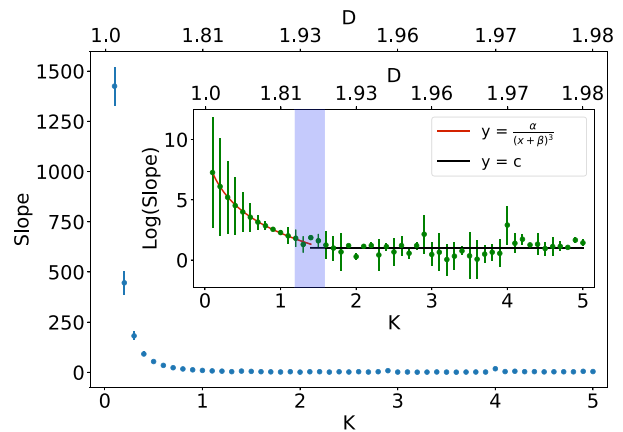


FIG. 3. The slope refers to the slope of the fitted line in the graphs such as in Fig. 2.  $K$  is shown on the lower  $x$  axis and the corresponding fractal dimension is shown in the upper  $x$  axis labeled as  $D$ . The inset shows the same data in a semi-log plot. The parameters for the fitting in the inset are  $\alpha = 12.71 \pm 0.48$ ,  $\beta = 0.11 \pm 0.01$ , and  $c = 1.02 \pm 0.10$ ; the shaded area denotes the region where both fitting functions overlap. The error bars were calculated using the fitting function and are one standard deviation.

#### IV. CONCLUSIONS

In this work, we have explored dynamic localization in one-dimensional systems, using the kicked rotor as a case scenario, in a wide dynamical range whose classical counterpart goes from regular to diffusive. The onset of classical chaos has been characterized via the fractal dimension of the phase space. This parameter has a straightforward interpretation as the portion of the phase space that shows a chaotic behavior vs the stable one. On the other hand, dynamical localization in the quantum realm is characterized by the relationship between the energy and localization of the wave function. As a result, we find that only when the system shows a classical diffusive character dynamical, localization emerges in accordance with previous results in different one-dimensional systems. However, in our case, we propose to use the slope of the energy vs the square of the localization length to characterize the aforementioned transition, thus finding a possible new parameter to quantitatively characterize the onset of quantum chaos.

Finally, our findings support previous explanations on the nature of dynamical localization due to quantum interference but only when the underlying classical dynamics present a diffusive character, thus helping to mitigate the initial thought that dynamical localization is a pure quantum effect based on its similitude with Anderson localization.

#### ACKNOWLEDGMENTS

We acknowledge Professor Felix M. Izrailev for comments and advice during the development of this work. In addition, we thank Dr. Marjan Mirahmadi for reading the manuscript and for helpful discussions.

#### AUTHOR DECLARATIONS

##### Conflict of Interest

The authors have no conflicts of interest to disclose.

#### DATA AVAILABILITY

The data that support the findings of this study are available from the corresponding author upon reasonable request.

#### APPENDIX A: FRACTAL DIMENSION CALCULATION

Following the box-counting method, to calculate the fractal dimension of a set of points, we place the set of points in question on a grid of squares and count the number of non-empty squares,  $N_0$ . Next, the set of points is scaled by a factor  $f$ , and we count the number of squares again,  $N_1$ . If the set of points were all of the points within some closed loop in two dimensions, then we would expect  $N_1 \approx N_0 f^2$ , as we know that the area scales with the square of the scaling factor (it will not be exact as the grid is not arbitrarily fine). In general, we would expect  $N_1 \approx N_0 f^D$ , where  $D$  is the fractal dimension.

Instead of dealing with just two data points, we can scale the set many times and plot the number of non-empty squares as a function of the scaling factor, as shown in Fig. 4. In that case, the number of non-empty squares is given by

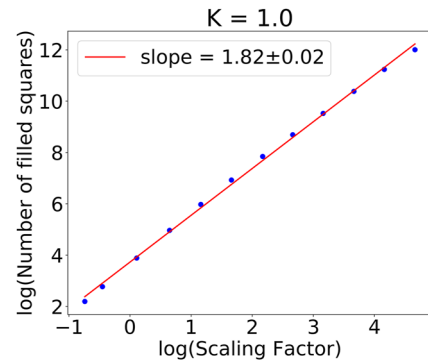


**FIG. 4.** Determining the fractal dimension for the phase space plot of the classical kicked rotor for  $K = 1$ . The slope of the fitted line gives us the fractal dimension.

$$N(f) = cf^D. \quad (\text{A1})$$

Thus, by plotting the data points in a log–log plot, we can simply fit a straight line as

$$\log(N(f)) = \log(cf^D) = D \log(f) + \log(c) \quad (\text{A2})$$

to the points, the slope of which will be the fractal dimension  $D$ . An example of this is given in Fig. 4.

#### APPENDIX B: NUMERICAL SIMULATIONS

In simulations of the quantum kicked rotor, the initial wave function is entirely localized in momentum space at 0 momentum, i.e.,

$$|\psi(t=0)\rangle = \sum_{n=-l}^l c_n(0)|n\rangle, \quad (\text{B1})$$

with  $c_0 = 1, c_{i \neq 0} = 0$ . The value of  $l$ , meaning the largest momentum state under consideration, is determined upon analyzing the eigenvalues of the  $\hat{U}$  matrix. In particular, we chose  $l$  such that at least 99% of their eigenvalues are within  $1 \pm 10^{-4}$ . Therefore, the matrix representing the operator is nearly unitary, as it should. Another way to check that the chosen basis is large enough is to run the simulation for the required number of kicks  $n$  and then check the extreme ends of  $|\psi(nT)\rangle$ . If the coefficients are 0 at the extremes, then we can be sure that the matrix was large enough, as the wave function never reached the boundary. As a result, all the results provided in our work are physically meaningful due to the proper unitary propagation carried out.

#### REFERENCES

- <sup>1</sup>B. V. Chirikov, *Phys. Rep.* **52**, 263 (1979).
- <sup>2</sup>J. M. Greene, *J. Math. Phys.* **20**, 1183 (1979).
- <sup>3</sup>G. Casati, B. V. Chirikov, F. M. Izrailev, and J. Ford, in *Stochastic Behavior in Classical and Quantum Hamiltonian Systems*, edited by G. Casati and J. Ford (Springer, Berlin, Heidelberg, 1979), pp. 334–352.
- <sup>4</sup>F. Benvenuto, G. Casati, A. S. Pikovsky, and D. L. Shepelyansky, *Phys. Rev. A* **44**, R3423 (1991).
- <sup>5</sup>D. L. Shepelyansky, *Phys. Rev. Lett.* **70**, 1787 (1993).
- <sup>6</sup>F. M. Izrailev, *Phys. Rep.* **196**, 299 (1990).

- <sup>7</sup>M. Khodas and S. Fishman, *Phys. Rev. Lett.* **84**, 2837 (2000).
- <sup>8</sup>S. Fishman, D. R. Grempel, and R. E. Prange, *Phys. Rev. Lett.* **49**, 509 (1982).
- <sup>9</sup>D. R. Grempel, R. E. Prange, and S. Fishman, *Phys. Rev. A* **29**, 1639 (1984).
- <sup>10</sup>F. M. Izrailev and D. L. Shepelyansky, *Theor. Math. Phys.* **43**, 553 (1980).
- <sup>11</sup>R. Lima and D. L. Shepelyansky, *Phys. Rev. Lett.* **67**, 1377 (1991).
- <sup>12</sup>M. Lepers, V. Zehnlé, and J. C. Garreau, *Phys. Rev. A* **77**, 043628 (2008).
- <sup>13</sup>J. E. Bayfield, S. Y. Luie, L. C. Perotti, and M. P. Skrzypkowski, *Phys. Rev. A* **53**, R12 (1996).
- <sup>14</sup>M. R. W. Bellermann, P. M. Koch, D. R. Mariani, and D. Richards, *Phys. Rev. Lett.* **76**, 892 (1996).
- <sup>15</sup>M. G. Raizen, F. L. Moore, J. C. Robinson, C. F. Bharucha, and B. Sundaram, *Quantum Semiclassical Opt.* **8**, 687 (1996).
- <sup>16</sup>F. L. Moore, J. C. Robinson, C. F. Bharucha, B. Sundaram, and M. G. Raizen, *Phys. Rev. Lett.* **75**, 4598 (1995).
- <sup>17</sup>P. Szriftgiser, H. Lignier, J. Ringot, J. C. Garreau, and D. Delande, *Commun. Nonlinear Sci. Numer. Simul.* **8**, 301 (2003), part of the Special Issue: Chaotic transport and complexity in classical and quantum dynamics.
- <sup>18</sup>M. G. Raizen, *Philos. Mag. B* **80**, 2109 (2000).
- <sup>19</sup>J. Mangaonkar, C. Vishwakarma, S. S. Maurya, S. Sarkar, J. L. MacLennan, P. Dutta, and U. D. Rapol, *J. Phys. B: At., Mol. Opt. Phys.* **53**, 235502 (2020).
- <sup>20</sup>A. Ullah, S. K. Ruddell, J. A. Currivan, and M. D. Hoogerland, *Eur. Phys. J. D* **66**, 315 (2012).
- <sup>21</sup>F. L. Moore, J. C. Robinson, C. Bharucha, P. E. Williams, and M. G. Raizen, *Phys. Rev. Lett.* **73**, 2974 (1994).
- <sup>22</sup>F. Saif, *Phys. Rep.* **419**, 207 (2005).
- <sup>23</sup>B. Gadway, J. Reeves, L. Krinner, and D. Schneble, *Phys. Rev. Lett.* **110**, 190401 (2013).
- <sup>24</sup>F. J. Dyson, *J. Math. Phys.* **3**, 140 (1962).
- <sup>25</sup>F. J. Dyson, *J. Math. Phys.* **3**, 157 (1962).
- <sup>26</sup>F. J. Dyson, *J. Math. Phys.* **3**, 166 (1962).
- <sup>27</sup>F. J. Dyson and M. L. Mehta, *J. Math. Phys.* **4**, 701 (1963).
- <sup>28</sup>F. J. Dyson, *J. Math. Phys.* **3**, 1191 (1962).
- <sup>29</sup>M. L. Mehta and F. J. Dyson, *J. Math. Phys.* **4**, 713 (1963).
- <sup>30</sup>M. L. Mehta, *Random Matrices*, 3rd ed. (Elsevier, 2004).
- <sup>31</sup>C. E. Porter, in *Statistical Theories of Spectra: Fluctuations: A Collection of Reprints and Original Papers/with an Introductory*, edited by C. E. Porter (Academic Press, New York, 1965), p. xv, 576.
- <sup>32</sup>I. Guarneri, G. Casati, and V. Karle, *Phys. Rev. Lett.* **113**, 174101 (2014).
- <sup>33</sup>F. Revuelta, R. Chacón, and F. Borondo, *Phys. Rev. E* **98**, 062202 (2018).
- <sup>34</sup>G. G. Carlo, J. Montes, and F. Borondo, *Phys. Rev. E* **105**, 014208 (2022).
- <sup>35</sup>D. S. Heinz-Otto Peitgen and H. Jürgens, *Chaos and Fractals* (Springer Science, 2004).
- <sup>36</sup>S. Strogatz, *Nonlinear Dynamics and Chaos*, 2nd ed. (Westview Press, 2015).
- <sup>37</sup>B. C. Yang, J. Pérez-Ríos, and F. Robicheaux, *Phys. Rev. Lett.* **118**, 154101 (2017).
- <sup>38</sup>D. K. Umberger and J. D. Farmer, *Phys. Rev. Lett.* **55**, 661 (1985).
- <sup>39</sup>S. E. Newhouse, "Topological entropy and Hausdorff dimension for area preserving diffeomorphisms of surfaces," *Astérisque* **51**, 323 (1978), [http://www.numdam.org/item/AST\\_1978\\_\\_51\\_\\_323\\_0/](http://www.numdam.org/item/AST_1978__51__323_0/).
- <sup>40</sup>F. Freistetter, *Celestial Mech. Dyn. Astron.* **78**, 211 (2000).
- <sup>41</sup>G. Benettin, D. Casati, L. Galgani, A. Giorgilli, and L. Sironi, *Phys. Lett. A* **118**, 325 (1986).
- <sup>42</sup>M. V. Berry, *J. Phys. A: Math. Gen.* **12**, 781 (1979).
- <sup>43</sup>V. Arnold, *Usp. Mat. Nauk* **18**, 91 (1963).
- <sup>44</sup>J. Moser, *On Invariant Curves of Area-Preserving Mappings of an Annulus* (Vandenhoeck & Ruprecht, 1962), Vol. 1.
- <sup>45</sup>R. Blümel and W. P. Reinhardt, *Chaos in Atomic Physics*, Cambridge Monographs on Atomic, Molecular and Chemical Physics (Cambridge University Press, 1997).